Journal of Materials Chemistry

Cite this: *J. Mater. Chem.*, 2012, **22**, 18583

www.rsc.org/materials

PAPER

Transformations and enhanced long-range ordering of mesoporous phenolic resin templated by poly(ethylene oxide-*b*-ε-caprolactone) block copolymers blended with star poly(ethylene oxide)-functionalized silsesquioxane (POSS)†

Jheng-Guang Li, Cheng-Yu Chung and Shiao-Wei Kuo*

Received 5th June 2012, Accepted 6th July 2012
DOI: 10.1039/c2jm33614f

In this study, we prepared ordered mesoporous phenolic resins templated by poly(ethylene oxide)-*b*-(ε-caprolactone) (PEO-*b*-PCL) diblock copolymers blended with a star PEO octa-functionalized polyhedral oligomeric silsesquioxane (PEO-POSS) homopolymer. Increasing the PEO-POSS content, and thereby increasing the PEO-to-PCL ratio in the template film, allowed us to tune and enhance the long-range order of the mesoporous phenolic resin. The increased pore size and the more ordered structure were accompanied by a narrower pore size distribution. In addition, we observed an ordered-to-ordered mesophase transition, from a bicontinuous gyroid to a hexagonally packed cylinder structure, upon blending with the star PEO-POSS homopolymer. We anticipate that this approach could be extended to the preparation of other large-pore, long-range-ordered mesoporous materials, such as silica and other metal oxides.

Introduction

The discovery of ordered mesoporous materials has attracted widespread research interest from academic and industrial communities, with their various applications in the fields of adsorption, separation, and nanoreactors for catalysis and confined synthesis.[1] The self-assembly of amphiphilic block copolymers as templates has been applied extensively for the structure-directed synthesis of mesoporous materials.[2,3] In the bulk state, diblock copolymers can form many different well-defined, self-assembled nanostructures, including lamellar, gyroid, hexagonally packed cylinders, and spherical structures.[4] The types of structures formed depends on the nature of the two immiscible polymer chains connected by covalent bonds, the relative volume fractions of the blocks, the total degree of polymerization, and the Flory–Huggins interaction parameter.[4]

Recently, systems based on diblock copolymers (A-*b*-B) blended with homopolymers (A or B) have attracted great interest in polymer science because of their unusual phase behavior.[5–10] Efficient blending in such a system depends critically on (i) the ratio of the molar weight of the additive homopolymer to that of the associated block of the copolymer and (ii) the volume fraction and miscibility of the additive homopolymer in the blend.[11–14] In addition, for an A-*b*-B/C blend system, two different outcomes are possible when homopolymer C is miscible with immiscible A-*b*-B segments.[15–23] Hydrogen bonding interactions of different strengths can lead to the formation of a variety of composition-dependent microphase separated structures.

Furthermore, the self-assembly of amphiphilic block copolymers in thermosets can be used to prepare ordered and disordered nanostructures.[24–27] Ordered mesoporous materials (*e.g.*, phenolic resin or carbon) having high surface areas, large pore volumes, and mechanical stability are attracting much attention for their potential applications in adsorption, separation, catalysis, photonics, and drug delivery. As a result, the formation of nanostructures in the blends of phenolic resins has been studied widely.[28–30] For example, Ikkala and Ruokolainen *et al.* prepared mesoporous phenolic resins from templates of poly(isoprene-*b*-2-vinyl pyridine) (PI-*b*-P2VP) and poly(styrene-*b*-4-vinyl pyridine) (PS-*b*-P4VP) diblock copolymers using hexamethylenetetramine (HMTA) as the curing agent.[31–33] Zheng *et al.* reported the formation of nanostructures in phenolic thermosets after curing novolac and poly(styrene-*b*-ethylene oxide) (PS-*b*-PEO) diblock copolymer with HMTA.[34] In all of the above studies, the phenolic resin was miscible with P4VP, P2VP, and PEO, stabilized through hydrogen bonding, but it was immiscible with PS or PI; that is, the C homopolymer was miscible with block B, but immiscible with block A.

In a previous study, we prepared a PEO-*b*-PCL (EC) diblock copolymer comprising two immiscible crystallizable blocks (PEO and PCL) that were both miscible with phenolic resin as a result of hydrogen bonding.[35] This system represents an A-*b*-B/C blend

Department of Materials and Optoelectronic Science, National Sun Yat-Sen University, Kaohsiung, 804, Taiwan. E-mail: kuosw@faculty.nsysu.edu.tw

† Electronic supplementary information (ESI) available. See DOI: 10.1039/c2jm33614f

in which the homopolymer C is miscible with both blocks A and B. Because the hydrogen bonds formed between PEO and the phenolic resin were significantly stronger than those between PCL and the phenolic resin,[36] we obtained a variety of composition-dependent nanostructures, including distorted lamellae and gyroid structures. An interesting closed-loop mesoporous structure existed in the phase diagram of the mesoporous phenolic resin templated by a PEO-*b*-PCL block copolymer, due to so-called "$\Delta\chi$" and "ΔK" effects.[37–41] In addition, we found that the long-range order of the structure increased when we templated the blends using a PEO-*b*-PCL diblock copolymer featuring a PCL block with a lower degree of polymerization. Thus, an increase in the relative PEO-to-PCL ratio in the block copolymers caused the C═O groups of the PCL block to compete with the ether oxygen atoms of PEO to form hydrogen bonds with the OH groups of the phenolic resin. Therefore, the key point for preparing mesoporous phenolic templated by PEO-*b*-PCL block copolymers is that the phenolic OH groups should undergo hydrogen bonding with the PCL C═O groups; the fraction of hydrogen-bonding PCL C═O groups, however, should not be too high as to form a miscible disordered system. As a result, the regular structures of the mesoporous phenolic resin templated by EC block copolymers are strongly dependent on the phenolic resin content and the relative PEO-to-PCL ratio.[35]

The synthesis of diblock copolymers is, however, a difficult and time-consuming approach toward varying the volume fractions of the block copolymer segments. From practical and economical points of view, physical blending of a diblock copolymer is a simpler and more effective method for preparing mesoporous materials, with greater versatility and flexibility. Zhao *et al.* used poly(ethylene-*b*-methyl methacrylate) (PEO-*b*-PMMA) and PEO-*b*-PS diblock copolymers as templates to prepare mesoporous silica samples through a simple evaporation-induced self-assembly (EISA) method, with the pore sizes reaching 12.1 and 22.6 nm when templated by the pure PEO-*b*-PMMA and PEO-*b*-PS diblock copolymers, respectively.[30,42] By simply blending with the homopolymers PMMA[42] and PS[43] as pore expanders, the pore sizes could be controlled from 8.6 to 22 nm and from 22.9 to 37.4 nm, respectively.

In this paper, we report the surprising enhancements in both the pore sizes and long-range order of mesoporous phenolic resins when templated by PEO-*b*-PCL diblock copolymers blended with star PEO octa-functionalized polyhedral oligomeric silsesquioxanes (PEO-POSS) as the homopolymer. We chose to use star PEO-POSS as the homopolymer because its degree of hydrogen bonding with phenolic resin is greater than those of linear homopolymers;[44,45] we anticipated that stronger intermolecular interactions might enhance the long-range order of the mesoporous structures.[46] With aging, we expected the cage-like POSS species to form larger silica clusters that can be also found in the walls of mesoporous silica.[47–51] In this study, we used Fourier transform infrared (FTIR) spectroscopy, small-angle X-ray scattering (SAXS), and transmission electron microscopy (TEM) to investigate the changes in phase morphology and the competing interactions within the mesostructures prepared from phenolic/PEO-*b*-PCL/PEO-POSS ternary blends.

Experimental

Materials

Monomethoxy-poly(ethylene glycol) with a molecular weight of 5000 (MPEG-5K) was obtained from Fluka and dried through azeotropic distillation with dry toluene. ε-Caprolactone (ε-CL, Acros) was purified by vacuum distillation over CaH_2; the distillation fraction collected at 96–98 °C (5 mm-Hg) was used in all polymerization reactions. Stannous(II) octoate [$Sn(Oct)_2$, Sigma] was used as received. CH_2Cl_2 was dried over CaH_2 prior to use. Star PEO-POSS was purchased from Hybrid Plastics (USA); the molecular weight of PEO-POSS was 5576 g mol^{-1} and there are eight arms on each POSS and 14 ethylene oxide units per arm. The phenolic was synthesized through a condensation reaction with H_2SO_4, producing an average molecular weight (M_n = 500) similar to those described in previous studies.[52–54] Diblock copolymers were readily prepared through the ring-opening polymerization of ε-CL in the presence of mPEG-5K and $Sn(Oct)_2$ as the catalyst.[55] The reaction mixtures were prepared by introducing the desired volume of ε-CL monomer into a silanized flask containing a pre-weighed amount of MPEG-5K under a N_2 atmosphere. One drop of $Sn(Oct)_2$ was added and then the flask was connected to a vacuum line, evacuated, sealed off, and heated at 130 °C. After 24 h, the resulting block copolymers were dissolved in CH_2Cl_2 and precipitated in an excess of cold *n*-hexane. The polymers were dried at 40 °C under vacuum. The properties of the diblock copolymers used in this study are summarized in Table 1.[35]

Synthesis of mesoporous phenolic resins

Phenolic resin, HMTA, PEO-*b*-PCL, and star PEO-POSS were dissolved in THF until the solution became homogeneous. The THF was evaporated slowly at room temperature and then the sample was vacuum-dried at 30 °C for 1 day. Curing of the samples was performed under the following temperature profile: 100 °C for 2 h, then 150 °C for 2 h, and then 190 °C for 2 h. The template polymers (PEO-*b*-PCL and PEO-POSS) have been removed by calcination at 330 °C at a rate of 1 °C min^{-1} in the absence of a protective gas of the crosslinked samples.

Characterization

Thermal analysis was performed using a TA Instruments Q-20 differential scanning calorimeter (DSC) operated at a heating rate of 20 °C min^{-1} and a cooling rate of 5 °C min^{-1} from

Table 1 Characterization of PEO-*b*-PCL diblock copolymers used in this study

Sample	Abbreviation	NMR M_n[a]	PDI[b]
$EO_{114}CL_{168}$	EC1	24 150	1.31
$EO_{114}CL_{130}$	EC2	19 820	1.29
$EO_{114}CL_{84}$	EC3	14 580	1.31

[a] Obtained by ^{1}H NMR spectra. [b] Obtained by GPC trace with DMF eluent of 0.6 ml min^{-1} and PS-standard calibration.

150 to −90 °C under N_2; the sample weighed between 5 and 10 mg. FTIR spectra of the samples were recorded using the conventional KBr disk method and a Bruker Tensor 27 FTIR spectrophotometer. SAXS data were recorded using a Nanostar U small-angle X-ray scattering system (Bruker, Germany) and Cu Kα radiation (40 kV, 35 mA). The *d* spacings were calculated using the formula $d = 2\pi/q$. Nitrogen sorption isotherms were measured at 77 K using an ASAP 2020 analyzer; prior to measurement, the sample was degassed under vacuum at 200 °C for at least 6 h. The Brunauer–Emmett–Teller (BET) method was used to calculate the specific surface areas. Using the Broekoff–de Boer (BdB) sphere model, the pore volumes and pore size distributions were derived from the adsorption branches of the isotherms; the total pore volumes were estimated from the adsorbed amount at a relative pressure (P/P_0) of 0.995. The calibration curve was recorded by using silica–alumina (part no. 004-16821-00) as a reference material and N_2 as the adsorption gas. TEM images were recorded using a JEOL 3010 microscope (Japan) operated at 200 kV; samples were prepared through solution-casting without thermal annealing. High-resolution scanning electron microscopy (HRSEM) images were recorded using a field emission JEOL JSM-6700F (Japan) instrument operated at 30 kV.

Results and discussion

Synthesis of mesoporous phenolic resins templated by PEO-*b*-PCL copolymer

Fig. 1 displays the SAXS patterns and TEM images of the mesoporous phenolic resins templated by different PEO-*b*-PCL block copolymers containing a fixed phenolic content (50 wt%), but various weight fractions of PCL. According to the positions of the first-order scattering peaks in Fig. 1(a), the average spacing between the neighboring microdomains decreased and the long-range order of the structure increased upon increasing the relative PEO-to-PCL ratio in the block copolymer. The quite weak and broad peak at 50 wt% phenolic content templated by the diblock copolymer EC1, as displayed in Fig. 1(a)-(i), indicates a distorted lamellar mesostructure, as confirmed by the TEM images in Fig. 1(b) and (c). The short-range order of the lamellar mesostructure was found at 50 wt% phenolic templated by diblock copolymer EC2, as demonstrated in Fig. 1(a)-(ii); this result was confirmed by the TEM images in Fig. 1(d) and (e). More interestingly, we observed a gyroid structure at 50 wt% phenolic templated by the diblock copolymer EC3; based on SAXS analysis, the intensity maximum appeared at a value of $6^{1/2}q^*$ of 0.26 nm^{-1} ($d = 24.1$ nm). The order reflections observed

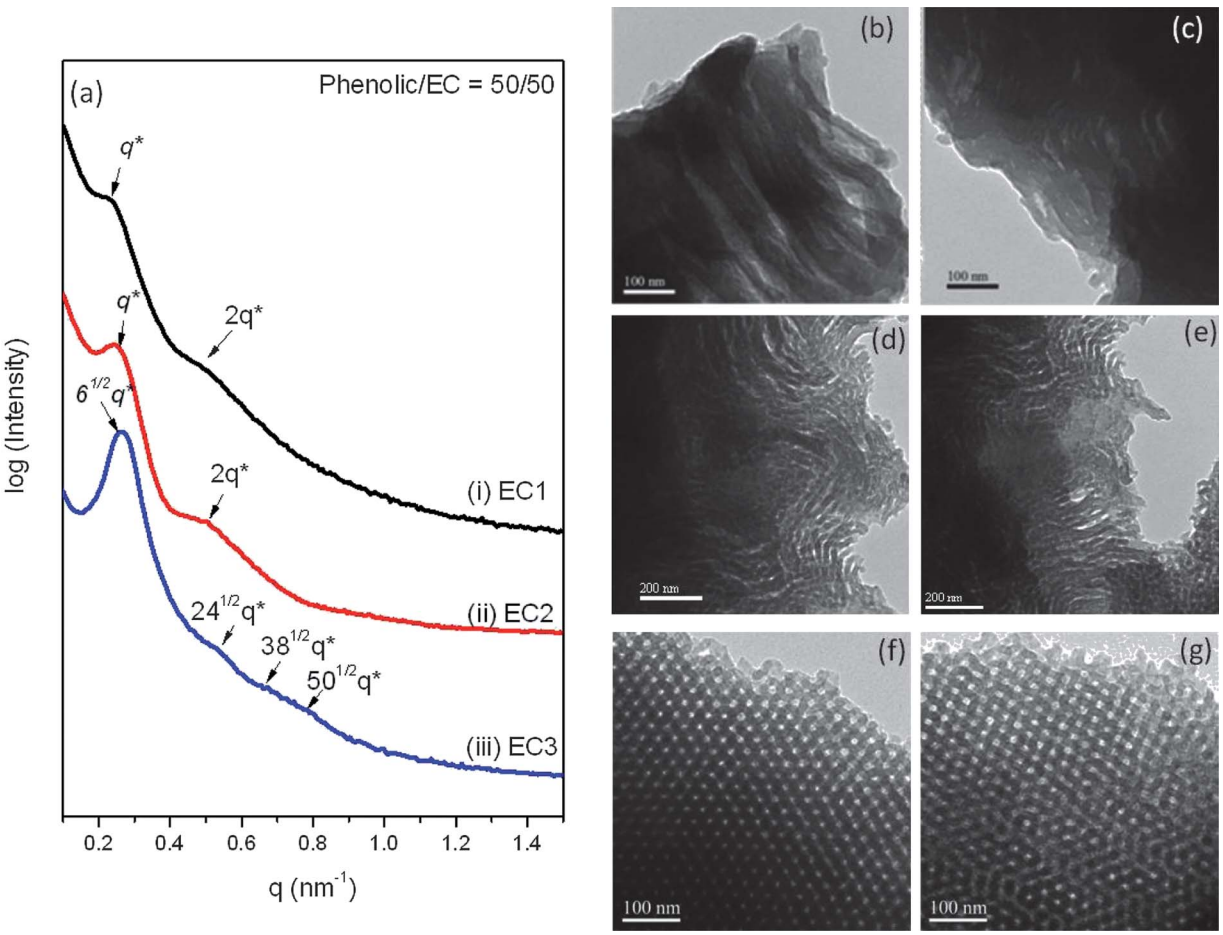

Fig. 1 (a) SAXS analyses and (b–g) TEM images of mesoporous phenolic resin structures containing a fixed phenolic resin content (50 wt%) and the templating block copolymers (b, c) EC1, (d, e) EC2, and (f, g) EC3.

at $24^{1/2}q^*$, $38^{1/2}q^*$, and $50^{1/2}q$ marked in Fig. 1(a)-(iii) are characteristic of a gyroid structure, which was confirmed by the TEM images in Fig. 1(f) and (g). The bicontinuous gyroid structure formed because the fraction of hydrogen-bonded C=O groups of PCL decreased upon increasing the PEO-to-PCL ratio, as evidenced by FTIR spectroscopic analysis.[35] In other words, the phenolic OH groups interacted with the PCL C=O groups to decrease the long-range order of the structure; these interactions increased the average size of the long-periodic structures in the mesoporous phenolic resin. As a result, the structures of the regular mesoporous phenolic resin templated by the EC block copolymers were strongly dependent on the relative PEO-to-PCL ratio. We observed, however, only distorted lamellar and bicontinuous gyroid structures (no cylindrical or spherical structures) because of the limited range of the PEO-to-PCL ratios in these three diblock copolymers. In a previous study, we obtained higher PEO-to-PCL ratios by using a PCL-*b*-PEO-*b*-PCL triblock copolymer in which the PEO weight fraction in the block copolymer was greater than 50 wt%, resulting in disordered spherical (micelle) structures.[35] This approach toward varying the volume fraction of the block copolymer segments through synthesis is, however, difficult and time-consuming; physical blending of a homopolymer into a diblock copolymer is a much simpler and more effective method of preparing mesoporous materials. In this study, we chose star PEO-POSS as the homopolymer to increase the relative PEO-to-PCL ratio and decrease the fraction of hydrogen-bonded PCL C=O groups.

DSC and FTIR spectroscopic analyses of phenolic/PEO-*b*-PCL/PEO-POSS ternary blends

Phenolic is totally miscible with PEO and PCL in the amorphous phase, due to inter-association hydrogen bonding between the OH groups of the phenolic and either the C=O group of the PCL or the ether oxygen atoms of the PEO.[36,55] In general, DSC analysis is a convenient method of determining the miscibility of polymer blends. The glass transition temperatures (T_g) of the pure phenolic, PEO, and PCL polymers used in this study were 66, –60, and −60 °C, respectively.[35,36] Fig. 2(A) displays conventional second-run DSC thermograms of various compositions of phenolic/EC2/PEO-POSS ternary blends (not cured with HMTA), recorded at a heating rate of 20 °C min^{-1}. The melting temperatures of both the PEO and PCL blocks disappeared for the phenolic/EC2 = 50/50 binary blend; decreases in melting temperatures result from morphological effects and the thermodynamic consequences of hydrogen bonding with phenolic resins.[56–60] In addition, we observed two glass transition temperatures for the phenolic/EC2 = 50/50 system and for the phenolic/EC2/PEO-POSS systems with different PEO-POSS contents, implying that they were immiscible in the amorphous phase as a result of so-called $\Delta\chi$ and ΔK effects,[36–40] because the phenolic interacted more favorably with the PEO than with the PCL. The higher and lower values of T_g of the phenolic–PEO and phenolic–PCL phases resulted from the inter-association equilibrium constant for phenolic OH groups and PEO ether oxygen atoms ($K_A = 264$) being greater than that for the OH groups of phenolic and the C=O groups of PCL ($K_A = 116$).[36] Interestingly, the peak for the melting temperature appeared for the phenolic/EC2/PEO-POSS = 50/50/10 system; its value shifted to higher temperature upon increasing the PEO-POSS content. The melting temperatures of PEO (70 °C) and PCL (60 °C) are very close. Initially, we suspected that the melting temperature of the phenolic/EC2/PEO-POSS = 50/50/10 system arose from the PEO phase and the increase in the PEO content. By taking into account the concept of competing equilibrium constants, however, the inter-association equilibrium constant for the OH···ether oxygen atom interaction is greater than the OH···O=C interaction. The strength of the OH···O=C interaction gradually decreased upon increasing the PEO content in these ternary blends. As a result, the PCL blocks were excluded to form their own domain and crystallization occurred, similar to our findings in a previous study of phenolic/PEO/PCL ternary blends.[36]

Fig. 2(B) presents the DSC thermograms of the phenolic/EC2/PEO-POSS ternary blends (not cured with HMTA) recorded under a slow cooling rate (5 °C min^{-1}) to determine the crystallization temperature. The peak temperature of the crystallization exotherm is defined as the freezing temperature (T_f); a higher value of T_f corresponds to a faster rate of crystallization. The value of T_f is associated with non-isothermal crystallization under a fixed cooling rate and displays a distinct correlation with the microdomain structure.[61–64] Clearly, at lower PEO-POSS contents (<10 wt%), the ternary blends exhibited only two glass transition temperatures, indicating an immiscible amorphous phase. Further increases in the PEO-POSS content (to >18 wt%) resulted in a relatively lower value of T_f (*ca.* −45 °C). These lower values of T_f were not evident for the PEO or PCL homopolymers, which appear at much larger undercooling. Chen *et al.*[61,62] reported that the degree of supercooling ($\Delta T = T_m^0 - T_f$, $T_m^0 =$ 75 °C) required to initiate crystallization in the lamellar microdomains ($\Delta T = 50$ °C) is comparable to that associated with the PCL homopolymer ($\Delta T = 42$ °C); exceedingly large undercoolings are required for crystallization in the cylindrical microdomains ($T_f = -50$ °C; $\Delta T = 125$ °C).[65] As a result, the

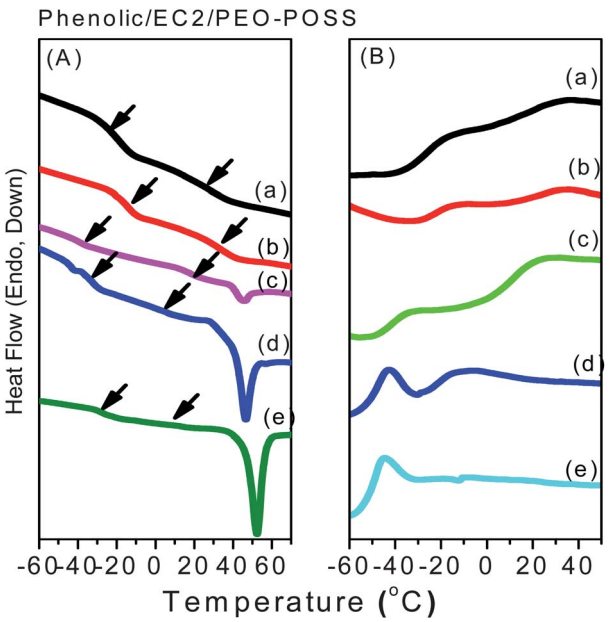

Fig. 2 DSC thermograms of phenolic/EC2/PEO-POSS ternary blends before calcination; (A) heating and (B) cooling scans of (a) 50/50/0, (b) 50/50/6, (c) 50/50/10, (d) 50/50/18, and (e) 50/50/26 ratios.

exotherm at a lower value of T_f (−45 °C) may have originated from the PCL block in a 2D cylindrical confinement (ΔT = 120 °C), because the lowest value of T_f of the PEO block in a 3D sphere confinement was −30 °C,[61] consistent with the heating scan in Fig. 2(A). In addition, the reversibility of the DSC thermograms was found for these systems.

Fig. 3 displays FTIR spectra recorded at room temperature in the OH, C=O, and ether vibration regions for a series of phenolic/EC3/PEO-POSS ternary blends containing a constant phenolic resin content of 50 wt%. In the phenolic/EC3 = 50/50 binary blend, the signal for the hydrogen-bonded OH groups appeared at 3350 cm^{-1}, reflecting specific OH···OH, OH···ether oxygen atoms, and OH···O=C hydrogen bonds. This band shifted to 3240 cm^{-1} (*i.e.*, lower wavenumber) upon increasing the PEO-POSS content in the blends (*i.e.*, increasing the PEO-to-PCL ratio) (Fig. 3(a)). This change arose from a switch from intermolecular OH···O=C hydrogen bonds to intermolecular OH···ether oxygen atom interactions, indicating that most of the hydrogen bonding occurred between the PEO ether oxygen atoms and the OH groups of the phenolic resin in the phenolic/EC3/PEO-POSS = 50/50/38 system.

Fig. 3(b) presents the FTIR spectra of the C=O stretching region (from 1650 to 1780 cm^{-1}) of these ternary blends at room temperature. The signal for the C=O stretching of the phenolic/EC3 = 50/50 system was split into two bands—for the free and hydrogen-bonded C=O groups at 1734 and 1708 cm^{-1}, respectively—that fitted well to the Gaussian function. Clearly, the fraction of hydrogen-bonded C=O groups decreased upon increasing the PEO-POSS content and, thereby, increasing the relative PEO-to-PCL ratio. This situation arose because the inter-association equilibrium constant for the OH···ether oxygen atom interaction (K_A = 264) was greater than that for the OH···O=C interaction (K_A = 116) at room temperature, based on the Painter–Coleman association model.[36,66,67]

Fig. 3(c) displays scale-expanded FTIR spectra in the range 1050–1140 cm^{-1} for our phenolic/EC3/PEO-POSS blends. With the formation of hydrogen bonds between the phenolic and the PEO, a band appeared at 1100 cm^{-1}; increasing the PEO-POSS content did not result in a shift of this band, indicating that the OH···ether oxygen atom interactions were not influenced by the PEO-POSS content. As a result, the fraction of hydrogen-bonded C=O groups decreased upon increasing the PEO-POSS content and, thereby, increasing the relative PEO-to-PCL ratio. Here, the molecular weight of the star PEO-POSS (each PEO segment = 585 g mol^{-1}) was significantly lower than the molecular weight of the PEO blocks (5000 g mol^{-1}) in the EC diblock copolymers that would have wet brush behavior;[5] therefore, we would expect the morphology to change upon increasing the content of the star PEO-POSS.

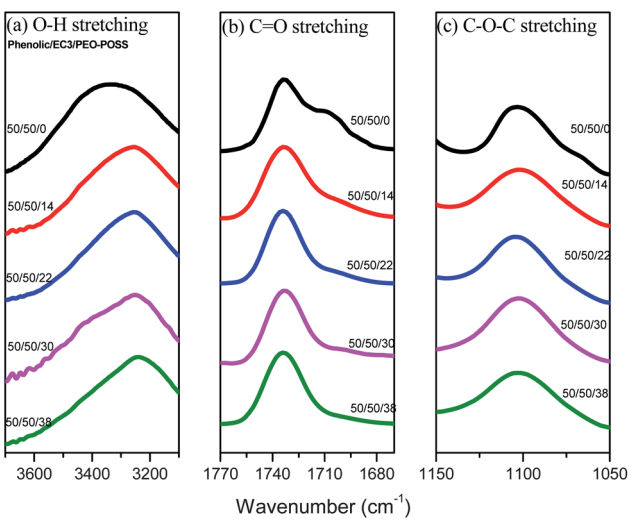

Fig. 3 FTIR spectra of phenolic/EC3/PEO-POSS systems before calcination, recorded at room temperature, displaying the (a) OH, (b) C=O, and (c) ether regions.

Synthesis of mesoporous phenolic resins templated by PEO-*b*-PCL/PEO-POSS blends

Fig. 4 displays the SAXS patterns obtained for the systems at 50 wt% phenolic content templated by the diblock copolymer EC1 in the presence of various PEO-POSS contents. The phenolic/EC1 = 50/50 system exhibited a near-lamellar and homogeneous morphology (Fig. 5(a)). According to the positions of the first-order scattering peaks in Fig. 4, the average spacing between the neighboring microdomains increased upon increasing the PEO-POSS content. We calculated the first-order scattering peaks in

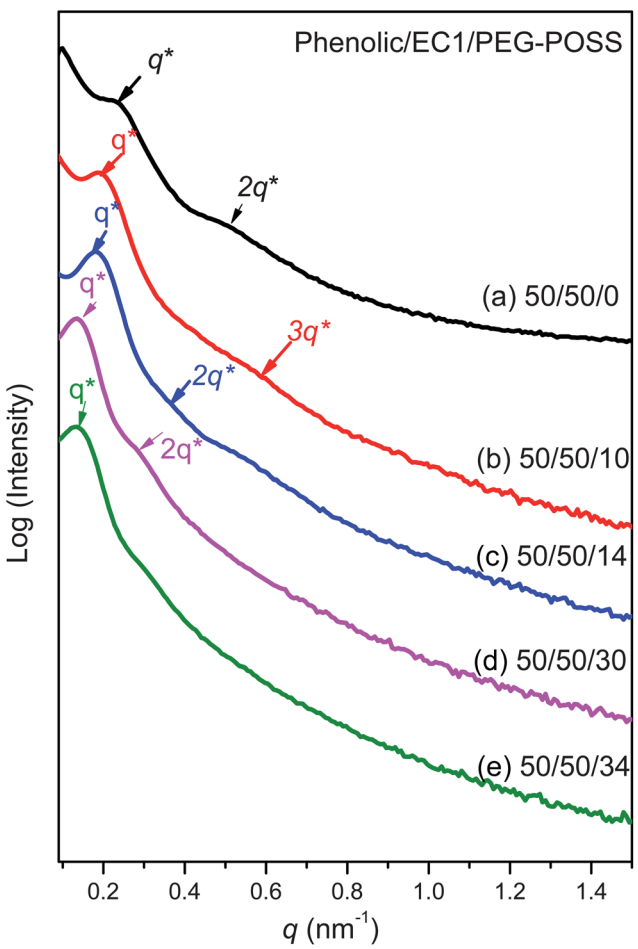

Fig. 4 Profiles of SAXS intensities of mesoporous phenolic resin structures obtained from templating EC1/PEO-POSS blends.

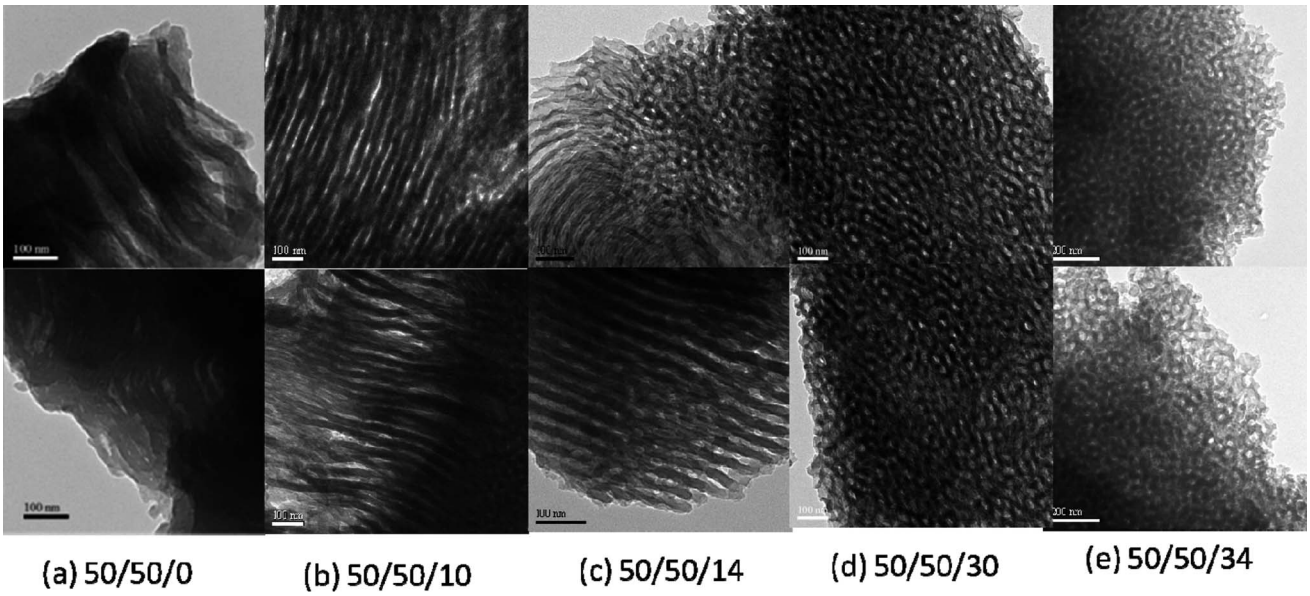

Fig. 5 TEM images of mesoporous phenolic structures obtained from phenolic/EC1/PEO-POSS blends.

Fig. 4(b) to be as large as 31.4 nm for the blend containing 10 wt % of PEO-POSS; this value was greater than that (26.4 nm) for the sample of the phenolic/EC1 = 50/50 system in the absence of PEO-POSS (Fig. 4(a)), suggesting a swollen mesostructure. The TEM images in Fig. 5(b) also reveal the lamellar structure. Further increasing the amount of PEO-POSS to 14 wt% led to a sharper first-order peak in the SAXS profile, indicating a long-range-ordered cylindrical mesostructure, which was also evident in the corresponding TEM image (Fig. 5(c)). The cell parameter of the first-order peak further increased to 34.8 nm, reflecting continuous structural expansion. Furthermore, we observed ultralarge *d*-spacings (46.1–47.9 nm) in the SAXS data when we further increased the content of PEO-POSS to 30–34 wt%, but these SAXS patterns implied that the cylindrical mesostructures had degenerated slightly. Distorted cylinders and defects in the mesostructure were also evident in the TEM images in Fig. 5(d) and (e). At our highest PEO-POSS content (34 wt%), the system contained insufficient phenolic resin to template the EC/PEO-POSS blend and formed a disordered structure.

The N_2-sorption isotherms of the mesoporous phenolic formed from a series of phenolic/EC1/PEO-POSS ternary blends containing a constant content of phenolic resin (50 wt%) behaved like representative type-IV curves with a sharp capillary condensation step in the relative pressure range of 0.85 to 0.95 (Fig. S1†). The mesoporous phenolic samples templated by the copolymer EC1 at a 50 wt% phenolic content in the absence of PEO-POSS exhibited a typical H_4-like hysteresis loop at values of P/P_0 from 0.4 to 0.9, indicating a common mesoporous structure with large, branched, lamellar pores. Increasing the PEO content resulted in all of the samples exhibiting a typical H_1-like hysteresis loop, characteristic of cylindrical mesopores. Table 2 summarizes the BET surface areas, pore volumes, and BJH pore sizes of the mesoporous phenolic materials. The total BET surface area and the total pore volume generally increased at lower PEO-POSS contents (<10 wt%), but decreased thereafter at higher PEO-POSS contents. Using the Harkins and Jura model,[68] we could not, however, determine the mean pore size for the system templated by the block copolymer EC1 at 50 wt% phenolic content in the absence of PEO-POSS (Fig. S1(b)†). For the mesoporous phenolic structures templated by EC1 blended with PEO-POSS contents of 10, 14, 30, and 34 wt%, the mean pore sizes measured from the adsorption branches were 17.3, 25.4, 35.8, and 33.8 nm, respectively. Thus, the mean pore size was strongly dependent on the PEO-POSS content, which varied the PEO-to-PCL ratio. Adding PEO-POSS enhanced both the pore sizes and the long-range order of the mesoporous phenolic resins at relatively low PEO contents. At relatively higher PEO-POSS contents (30 and 34 wt% PEO-POSS), however, the distribution of mean pore sizes broadened because the system contained insufficient phenolic resin to template the EC/PEO-POSS system and, thereby, formed disorder structures, consistent with our SAXS and TEM analyses. As a result, increasing the PEO-to-PCL ratio is the key factor affecting the preparation of mesoporous phenolic at certain phenolic contents.

Next, we turned our attention toward the mesoporous phenolic resins templated by the diblock copolymer EC2 (with a higher PEO-to-PCL ratio than that of EC1) at various PEO-POSS contents. Fig. 6 and 7 summarize the SAXS patterns and TEM images, respectively, of the mesoporous phenolic resins templated by the various PEO-POSS contents in the fixed phenolic/EC2 = 50/50 system. For the samples containing 0, 6, 10, 18, and 26 wt% PEO-POSS contents, the first peaks in the SAXS patterns in Fig. 6 corresponded to average spacings of 26.0, 26.8, 29.4, 36.8, and 34.0 nm, respectively, between neighboring microdomains. Similar to the systems templated by the block copolymer EC1, the average spacing between the neighboring microdomains increased upon increasing the PEO-POSS content to 18 wt%, but then decreased at a 26 wt% PEO-POSS content. In Fig. 6(a), the two major scattering peaks at values of q of 0.0245, and 0.0490 A^{-1}, with a peak ratio of 1 : 2, indicate a lamellar structure, which was further confirmed by TEM analysis (Fig. 7(a)). The first-order scattering peaks in Fig. 6(b) and (c)

Table 2 Textural properties of the mesoporous phenolic resin structures

Sample Phenolic/EC	d (nm)[a]	Pore size (nm)	S_{BET} (m^2 g^{-1})[b]	S_M (m^2 g^{-1})[b]	Pore volume (cm^3 g^{-1})	Micropore volume (cm^3 g^{-1})
Phenolic/EC1/PEO-POSS						
50/50/0	26.2	—	193	92	0.17	0.04
50/50/10	31.4	17.4	208	74	0.34	0.01
50/50/14	34.8	25.4	222	54	0.49	0.02
50/50/30	46.1	35.8	170	48	0.40	0.01
50/50/34	47.9	33.8	171	17	0.41	0.04
Phenolic/EC2/PEO-POSS						
50/50/0	26.0	13.3	391	203	0.43	0.09
50/50/6	26.8	15.3	428	207	0.48	0.10
50/50/10	29.4	17.3	468	239	0.54	0.11
50/50/18	36.8	25.5	467	219	0.46	0.10
50/50/26	34.0	22.5	455	209	0.48	0.10
Phenolic/EC3/PEO-POSS						
50/50/0	22.1	17.6	328	92	0.60	0.04
50/50/14	25.2	19.4	339	83	0.66	0.04
50/50/22	26.0	19.8	349	85	0.61	0.04
50/50/30	26.8	20.0	432	146	0.62	0.06
50/50/38	34.0	17.2	437	147	0.65	0.07

[a] The d-spacing values were calculated by the formula $d = 2\pi/q^*$. [b] S_{BET} and S_M are the total BET surface area and micropore surface area calculated from the t-plots, respectively.

were as large as 26.8 and 29.4 nm for the blends containing 6 and 10 wt% of PEO-POSS, respectively; these values are larger than that (26.0 nm) for the sample from the phenolic/EC2 = 50/50 system in the absence of PEO-POSS (Fig. 6(a)), suggesting swollen mesostructures. In addition, the TEM images in Fig. 7(b) and (c) reveal enhancements in the long-range ordering of the lamellar mesostructures relative to that of the phenolic/EC2 = 50/50 system in the absence of PEO-POSS (Fig. 7(a)). Further increasing the amount of PEO-POSS to 18 wt% resulted in the SAXS profile exhibiting organized peaks with a peak ratio of $1 : 3^{1/2} : 2$, indicating hexagonally packed cylinders, as imaged in Fig. 7(d); the cell parameter of the first-order peak increased further to 36.8 nm, reflecting a continuous structural expansion. The first-order peak of the system at 26 wt% PEO-POSS, however, shifted toward higher values of q, corresponding to a shrinkage of the cylinder spacing (34.0 nm). This system also exhibited long-range order with a peak ratio of $1 : 3^{1/2} : 2$; its TEM images are displayed in Fig. 7(e).

In Fig. S2,† the N_2-sorption isotherms of the mesoporous phenolic structures obtained from a series of phenolic/EC2/PEO-POSS ternary blends containing a constant content of phenolic resin (50 wt%) exhibited representative type-IV curves with a sharp capillary condensation step in the relative pressure range from 0.85 to 0.95. The results are similar to those of the system templated by the copolymer EC1. The mesoporous phenolic samples templated by the copolymer EC2 at a 50 wt% phenolic content in the absence of PEO-POSS exhibited a typical H_4-like hysteresis loop. Increasing the PEO content resulted in all of the samples exhibiting a typical H_1-like hysteresis loop, characteristic of cylindrical mesopores. Table 2 summarizes the BET surface areas, pore volumes, and BJH pore sizes of these mesoporous phenolic materials. The total BET surface area and the total pore volume generally increased upon increasing the PEO-POSS content to 10 wt%, but then decreased thereafter at higher PEO-POSS contents. Based on the Harkins and Jura model, the mean pore sizes for the mesoporous phenolic samples templated

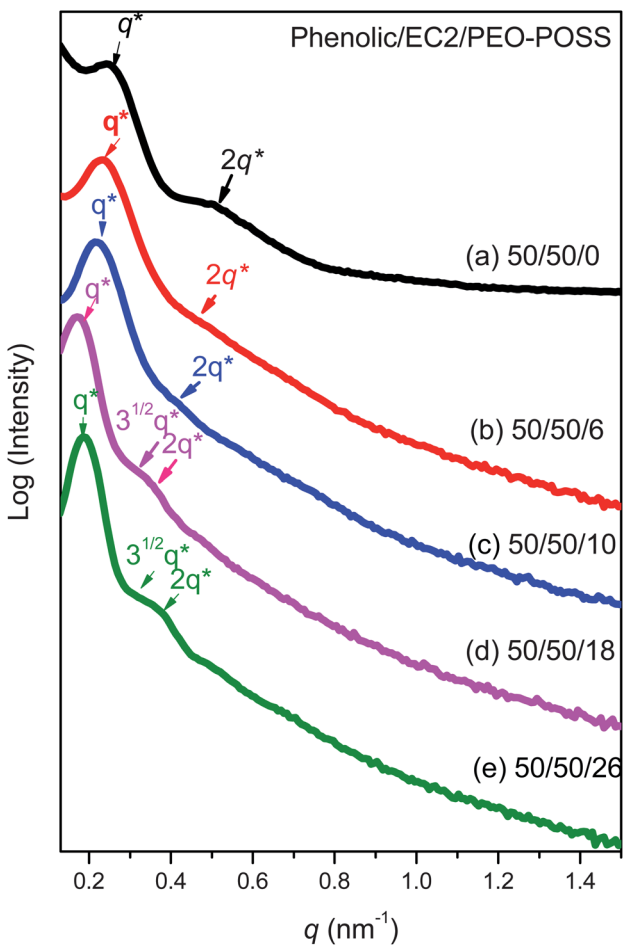

Fig. 6 Profiles of SAXS intensities of mesoporous phenolic resin structures obtained from templating EC2/PEO-POSS blends.

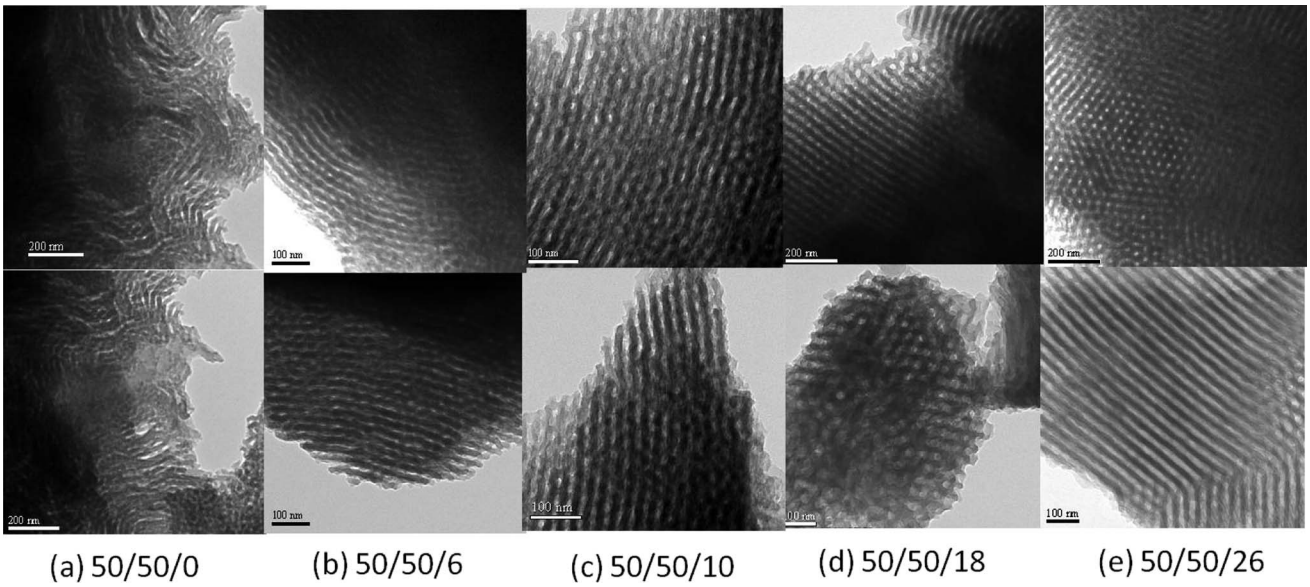

Fig. 7 TEM images of mesoporous phenolic structures obtained from phenolic/EC2/PEO-POSS blends.

by EC2 blended with PEO-POSS contents of 0, 6, 10, 18, and 26 wt%, measured from the adsorption branches, were 13.3, 15.3, 17.3, 25.5, and 22.5 nm, respectively. Thus, the mean pore size was strongly dependent on the PEO-POSS content, which varied the PEO-to-PCL ratio. Adding PEO-POSS increased both the pore sizes and the long-range order of the mesoporous phenolic resins at relatively low PEO contents (<18 wt%). At a relatively high PEO-POSS content of 26 wt%, however, the pore size decreased, consistent with the SAXS analysis data.

Next, we studied the mesoporous phenolic resin samples templated by the diblock copolymer EC3 (containing the highest PEO-to-PCL ratio) at various PEO-POSS contents. Fig. 8 and 9 summarize the SAXS patterns and TEM images, respectively, of the mesoporous phenolic resins templated by different PEO-POSS contents in the fixed phenolic/EC3 = 50/50 system. We observed an ordered bicontinuous gyroid structure for the phenolic/EC3 = 50/50 system in the absence of PEO-POSS, based on the SAXS profile in Fig. 8(a) and the TEM images in Fig. 9(a). For the samples containing PEO-POSS contents of 0, 14, 22, 30, and 38 wt%, the first peaks in the SAXS patterns in Fig. 8 correspond to average spacings of 22.1, 25.2, 26.0, 26.8, and 34.0 nm, respectively, between the neighboring microdomains. Similar to the systems templated by the block copolymer EC1, the average spacing between the neighboring microdomains increased upon increasing the PEO-POSS content. Most interestingly, when the PEO-POSS content was 22 wt%, the SAXS profile exhibited organized peaks having a peak ratio of $1 : 3^{1/2} : 2$, indicating hexagonally packed cylinders, which were also evident in Fig. 9(c). For this system, the cell parameter of the first-order peak increased to 26.0 nm, reflecting a continuous structural expansion. We found an ordered–ordered mesophase transition in this example of a system templated by the block copolymer EC3. Furthermore, when the PEO-POSS content increased further, the SAXS patterns of the samples prepared at 30 and 34 wt% PEO-POSS implied that the cylindrical mesostructures had degenerated slightly; distorted cylinders and defects in the mesostructure were also evident in the TEM images in Fig. 9(d) and (e). At higher PEO-POSS contents (30–38 wt%), insufficient phenolic

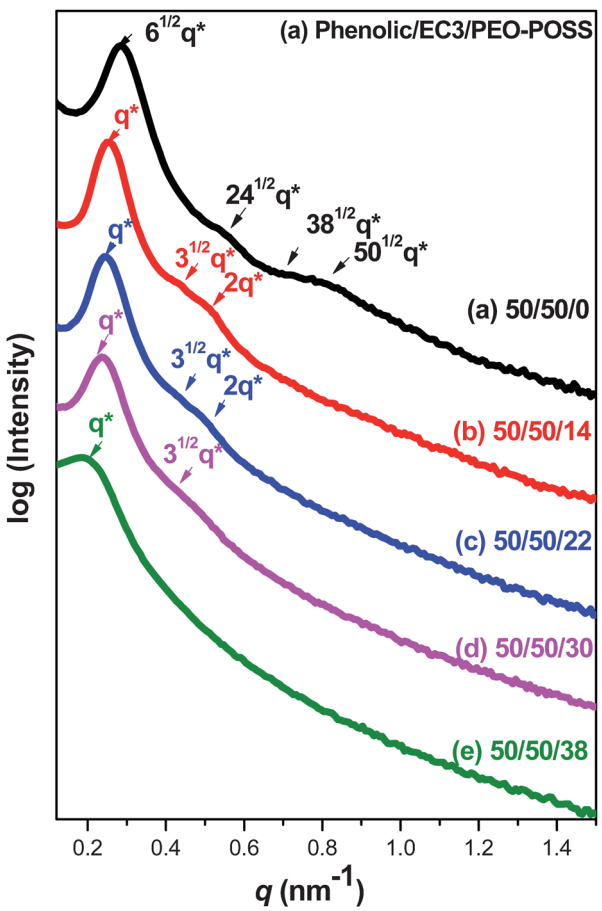

Fig. 8 Profiles of the SAXS intensities of mesoporous phenolic resin structures obtained from templating EC3/PEO-POSS blends.

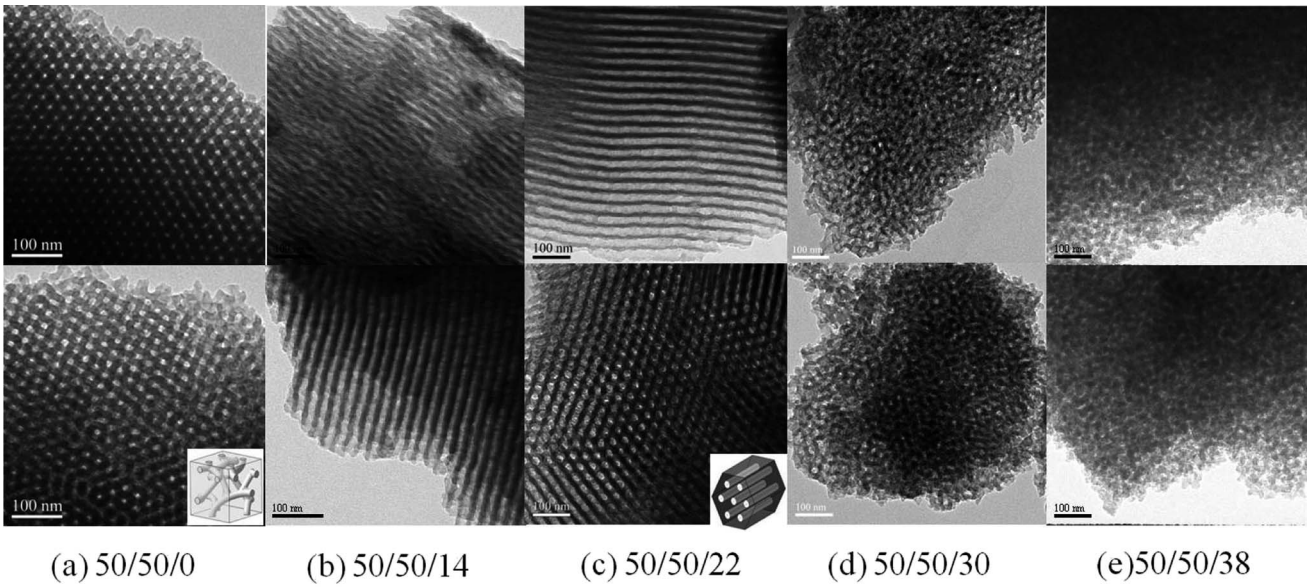

Fig. 9 TEM images of the mesoporous phenolic structures obtained from phenolic/EC3/PEO-POSS blends.

resin was present to template the EC3/PEO-POSS system, which, thereby, formed a disordered structure, similar to those templated by the EC1/PEO-POSS mixtures.

In Fig. S3,† the N_2-sorption isotherms of the mesoporous phenolic samples obtained from a series of phenolic/EC3/PEO-POSS ternary blends containing a constant phenolic resin

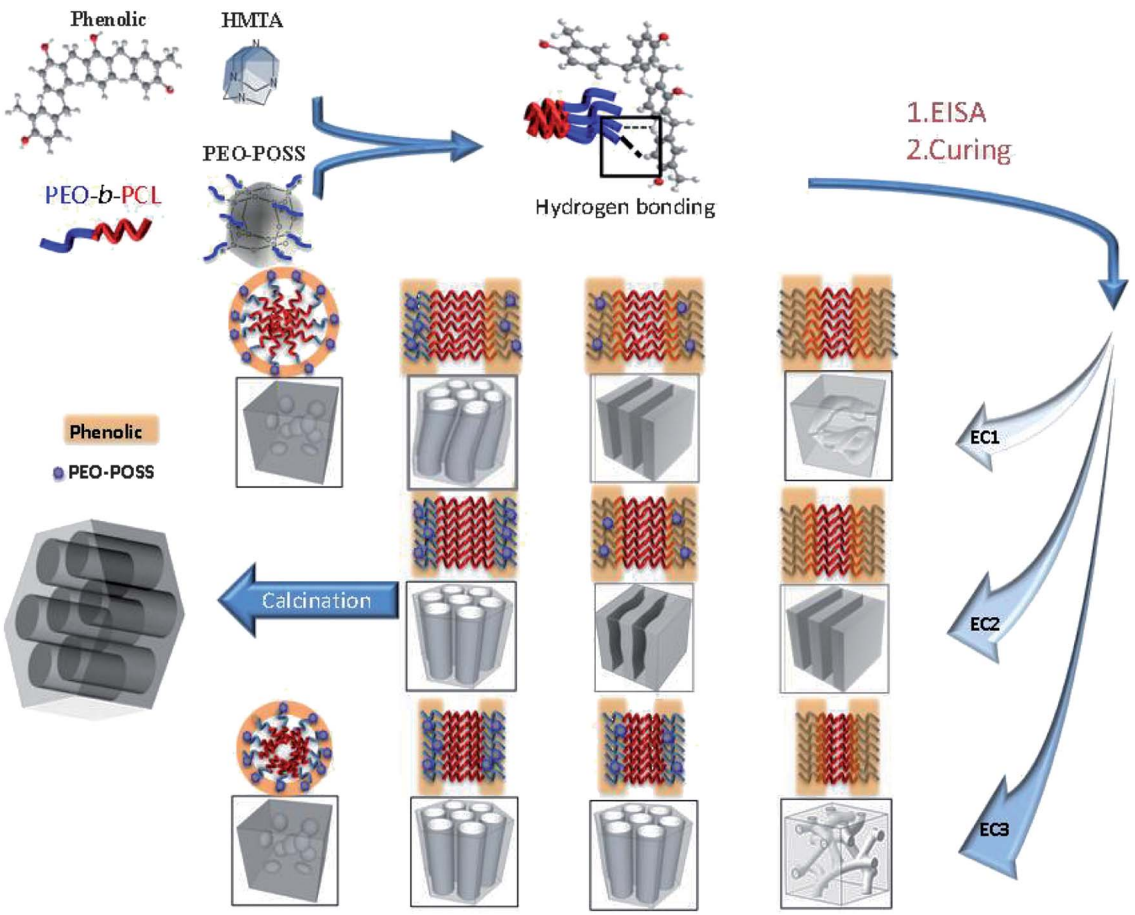

Scheme 1 Preparation and morphological changes of mesoporous phenolic resins templated by PEO-*b*-PLC/PEO-POSS blends with increasing PEO-POSS content.

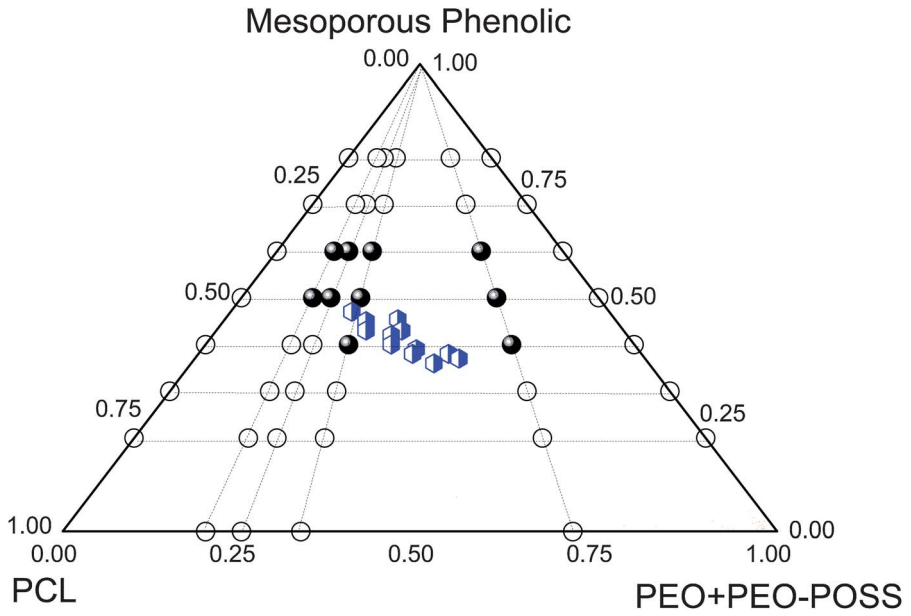

Fig. 10 Phase diagram of mesoporous phenolic resin from template by EC/PEO-POSS blends, the open circles represent disordered structure, the full circles represent regular mesoporous structure templated by pure EC diblock copolymer and the hexagonal symbols represent regular mesoporous structure templated by EC/PEO-POSS blends.

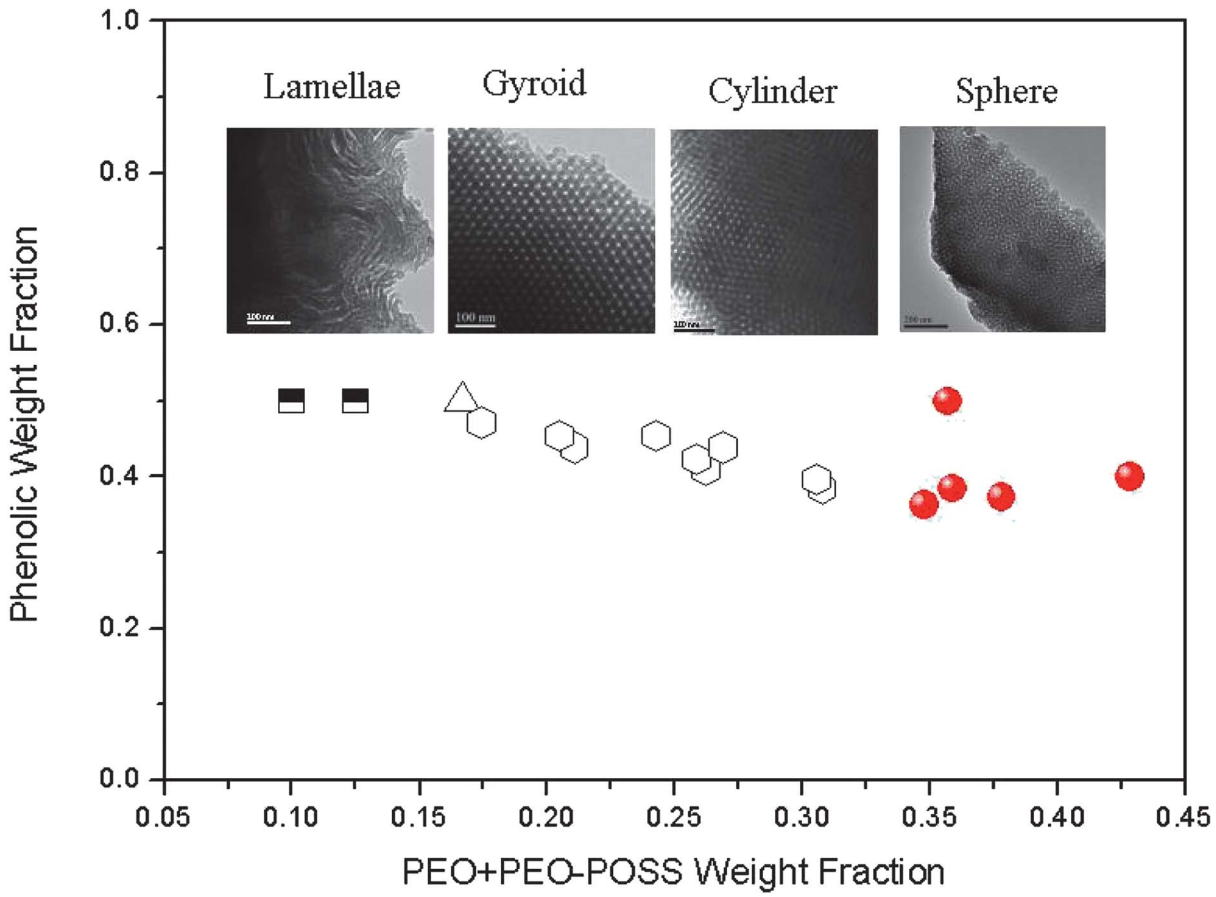

Fig. 11 Scale expanded phase diagram of phenolic/EC/PEO-POSS with different PEO + PEO-POSS weight fractions at phenolic resin content (*ca.* 0.35–0.5), the black and white symbols represent lamellae, triangle symbols represent gyroids, hexagonal symbols represent cylinders, circle symbols represent spherical mesoporous structures.

content (50 wt%) behaved like representative type-IV curves with a sharp capillary condensation step in the relative pressure range from 0.85 to 0.95. The mesoporous phenolic samples templated by the copolymer EC3 at a 50 wt% phenolic content exhibited a typical H_4-like hysteresis loop. Table 2 summarizes the BET surface areas, pore volumes, and BJH pore sizes of these mesoporous phenolic materials. The total BET surface area and the total pore volume generally increased upon increasing the PEO-POSS content to 30 wt%, but decreased thereafter. Based on the Harkins and Jura model, the mean pore sizes for the mesoporous phenolic structures templated by EC3 blended with PEO-POSS contents of 0, 14, 22, 30, and 38 wt%, measured from the adsorption branches, were 17.6, 19.4, 19.8, 20.0, and 17.2 nm, respectively. Thus, the mean pore size was strongly dependent on the PEO-POSS content, which varied the PEO-to-PCL ratios. Adding PEO-POSS increased both the pore sizes and the long-range order of the mesoporous phenolic resins at relatively low PEO contents (<30 wt%). At a relatively high PEO-POSS content (38 wt%), however, the pore size decreased, consistent with the SAXS analysis data.

Scheme 1 summarizes the detailed morphological changes that occurred in the mesoporous phenolic resin upon increasing the PEO-POSS content in the templating PEO-*b*-PCL/PEO-POSS blends. In addition, the phase diagram of the mesoporous phenolic templated by the EC/PEO-POSS block copolymers based on the SAXS patterns and TEM images is summarized in Fig. 10. Clearly, only distorted lamellar (EC1, EC2) and bicontinuous gyroid (EC3) structures (no cylindrical or spherical structures) were templated by the pure PEO-*b*-PCL diblock copolymers, due to the limited PEO-to-PCL ratios in our three diblock copolymers in Scheme 1. After blending with the PEO-POSS homopolymer, we observed long-range-ordered cylindrical morphologies, such as those of the phenolic/EC2/PEO-POSS = 50/50/26 and phenolic/EC3/PEO-POSS = 50/50/22 systems, as a result of increasing the PEO-to-PCL ratio. Most importantly, the short-range order of the mesoporous phenolic resin structures, such as those templated by the diblock copolymers EC1 and EC2, was enhanced after blending with the star PEO-POSS homopolymer (at certain contents) in terms of larger pore sizes and greater long-range-ordering of the mesoporous phenolic resin structures. We also found an ordered–ordered mesophase transition, from a bicontinuous gyroid to a hexagonally packed cylinder structure, when templating with the block copolymer EC3 blended with the star PEO-POSS homopolymer. Fig. 11 summarizes the scale expanded phase diagram of phenolic/EC/PEO-POSS with different PEO weight fractions. Clearly, a mesoporous morphology was found from lamellar, gyroid, hexagonally packed cylinders, and finally to spherical structures with the increase of the PEO weight fraction in this ternary blend, which is similar to a typical block copolymer phase diagram.[4] Therefore, we synthesized the PCL-*b*-PEO-*b*-PCL triblock copolymer to increase the PEO weight fraction in the block copolymer (>50 wt% PEO) and disordered spherical micelles were found by templated by PCL-*b*-PEO-*b*-PCL triblock copolymers.[35] We know that the synthesis of diblock copolymers is a difficult and time-consuming method for varying the volume fraction of block copolymer segments. Simple physical blending of homopolymers into diblock copolymers is a more effective method of mediating mesoporous materials, with greater versatility and flexibility to obtain different mesoporous structures (such as cylindrical morphology in this study) and to enhance the long-range order and pore sizes of mesoporous structures. Here, we must emphasize that the changing of the PEO fraction by using star PEO-functionalized POSS block copolymers is different from the synthesis of PEO-*b*-PCL triblock by controlling the PEO molecular weight since block copolymers would have short-range attraction by their covalent bonds. The phase diagram in Fig. 10 and 11 only suggested the possible mechanism for this block copolymer/homopolymer template for mesoporous phenolic resin.

Synthesis and morphology of mesoporous carbon

Mesoporous phenolic resin thin films and mesoporous carbon have applications in various fields. Fig. 12 displays TEM and SEM images of the gyroid and cylinder mesoporous carbon samples pyrolyzed from our mesoporous phenolic resin structures obtained from the phenolic/EC3 = 50/50 and phenolic/EC3/PEO-POSS = 50/50/22 systems. Fig. 12(a) and (b) present TEM images and corresponding Fourier diffractograms revealing that the mesoporous gyroid carbon had a high degree of periodicity over large domains. These images provide views from the [311] and [111] directions of the gyroid phenolic resin

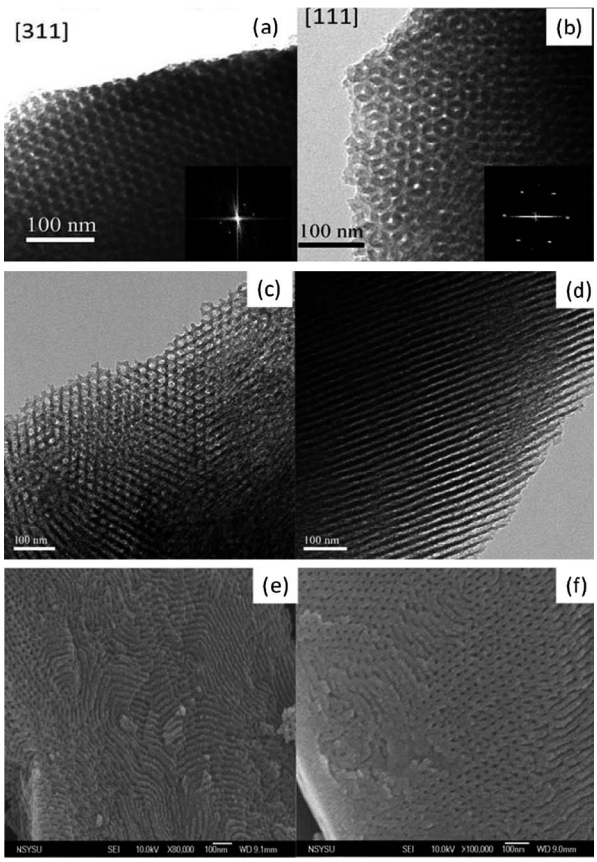

Fig. 12 (a and b) TEM images of gyroid mesoporous carbon structures pyrolyzed from the phenolic/EC3 = 50/50 system. (c and d) TEM images and (e and f) field-emission SEM images of cylindrical mesoporous carbon structures pyrolyzed from the phenolic/EC3/PEO-POSS = 50/50/22 system at 800 °C.

obtained from the phenolic/EC3 = 50/50 system calcined at 800 °C under N_2.[35,69] Fig. 12(c) and (d) display TEM images of the hexagonally packed cylindrical mesoporous carbon structure obtained from the phenolic/EC3/PEO-POSS = 50/50/22 system calcined at 800 °C under N_2. The transformation of the mesoporous carbon from a gyroid to a cylinder structure upon increasing the PEO-POSS content was also evident in the FE-SEM measurements presented in Fig. 12(e) and (f), which reveal uniform and regularly aligned mesopores throughout the whole film, suggesting the top view of a highly ordered hexagonal cylindrical mesostructure over a large domain.

Fig. 13(a) and (c) reveal the texture of the mesoporous carbon structures, as characterized by N_2 sorption isotherm experiments and the corresponding N_2 adsorption/desorption isotherms and pore size distributions. The gyroid and cylinder mesoporous carbon structures were also typical mesoporous materials; they exhibited representative type-IV isotherms, with H_1 hysteresis loops according to the IUPAC classification.[70] These isotherms suggest that the initial uniform, large, cylindrical pores were retained after pyrolysis. Furthermore, sharp steps occurred for these samples at relative pressures from 0.45 to 0.85, indicating the complete filling of the uniform mesopores by capillary forces. Compared with the gyroid (17.6 nm) and cylinder (19.8 nm) mesoporous phenolic resin structures, the mean pore sizes measured from the adsorption branches decreased to 11.0 nm (Fig. 13(b)) and 13.9 nm (Fig. 13(d)), respectively. The BET surface areas of the gyroid and cylindrical mesoporous carbon structures (Table S1†) were 858 and 749 $m^2\ g^{-1}$, respectively—much larger than those of both corresponding mesoporous phenolic resin structures, due to the removal of carbon, hydrogen, and oxygen atoms from the mesoporous matrix during pyrolysis. This process was primarily responsible for introducing the micropores; that is, the micropores were generated during the carbonization process. Therefore, the *d*-spacings of the mesoporous gyroid and cylindrical carbon structures became as large as 18.6 and 22.1 nm, respectively, reflecting shrinkages of 21 and 15% of their respective polymer frameworks. In general, the pore sizes of the mesoporous carbon structures are limited by the use of copolymers with low molecular weights. Employing an ordered mesoporous silica, such as SBA-15 (ref. 3 and 71) or KIT-6,[72] as a hard template can replicate carbon systems with ordered mesostructures and large porosity; that approach was a breakthrough in the area of mesostructured materials.[73] In this study, we increased the pore sizes of the ordered mesoporous carbon structures to 13.9 nm through simple blending with the homopolymer PEO-POSS. Here, we ignore the POSS molecules after calcination since the Si–O cage content from POSS is very low (<1.5 wt%) in this diblock copolymer/homopolymer template for mesoporous carbon.

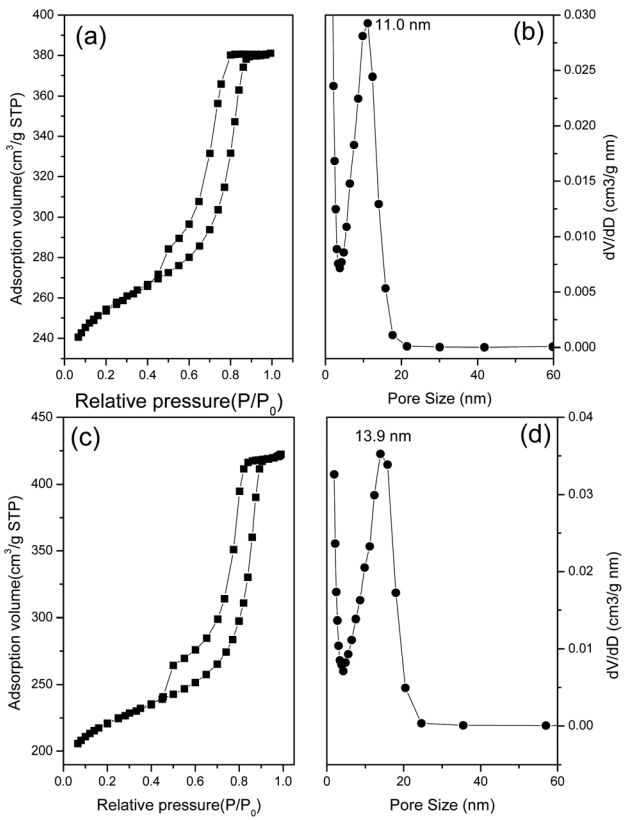

Fig. 13 (a and c) N_2 adsorption/desorption isotherms and (b and d) pore size distribution curves of gyroid mesoporous carbon structures pyrolyzed from the (a and b) phenolic/EC3 = 50/50 and (c and d) phenolic/EC3/PEO-POSS = 50/50/22 systems.

Conclusions

We have systematically examined the effect of a star PEO-POSS homopolymer as an additive in the PEO-*b*-PCL block copolymer template on the morphology of mesoporous phenolic resin structures. The star PEO-POSS homopolymer significantly increased both the pore size and the long-range order of the resulting mesoporous phenolic films. Using this approach, highly ordered mesoporous phenolic films with narrow pore size distributions are readily prepared using block copolymer/homopolymer blends as templates. Because of their large surface areas, pore sizes, and pore volume, the resulting large-pore mesoporous carbon structures might have potential applications in chemical sensors and fuel cells.

Acknowledgements

This study was supported financially by the National Science Council, Taiwan, Republic of China, under contracts NSC 100-2221-E-110-029-MY3 and NSC 100-2628-E-110-001.

Notes and references

1 J. Y. Ying, C. P. Mahnert and M. S. Wong, *Angew. Chem., Int. Ed.*, 1999, **38**, 56.
2 P. Yang, D. Y. Zhao, D. I. Margolese, B. F. Chmelka and G. D. Stucky, *Chem. Mater.*, 1999, **11**, 2813.
3 D. Y. Zhao, J. Feng, Q. Huo, N. Melosh, G. H. Fredrickson, B. F. Chmelka and G. D. Stucky, *Science*, 1998, **279**, 548.
4 J. Rodriguez-Hernandez, F. Checot, Y. Gnanou and S. Lecommandoux, *Prog. Polym. Sci.*, 2005, **30**, 691.
5 T. Tanaka, H. Hasegawa and T. Hashimoto, *Macromolecules*, 1991, **24**, 240.
6 Y. K. Han, E. M. Pearce and T. K. Kwei, *Macromolecules*, 2000, **33**, 1321.
7 M. Jiang and H. K. Xie, *Prog. Polym. Sci.*, 1991, **16**, 977.
8 W. V. Zoelen, G. A. V. Ekenstein, O. Ikkala and G. T. Brinke, *Macromolecules*, 2006, **39**, 6574.
9 Y. Matsushita, *Macromolecules*, 2007, **40**, 771.

10 P. Huang, L. Zhu, S. Z. D. Cheng, Q. Ge, R. P. Quirk, E. L. Thomas, B. Lotz, B. S. Hsiao, L. Z. Liu and F. J. Yeh, *Macromolecules*, 2001, **34**, 6649.
11 J. Bodycomb, D. Yamaguchi and T. Hashimoto, *Macromolecules*, 2000, **33**, 5187.
12 K. I. Winey, E. L. Thomas and L. J. Fetters, *Macromolecules*, 1992, **25**, 422.
13 S. W. Kuo, *Polym. Int.*, 2009, **58**, 455.
14 N. Hameed and Q. Guo, *Macromolecules*, 2008, **41**, 7596.
15 H. F. Lee, S. W. Kuo, C. F. Huang, J. S. Lu, S. C. Chan, C. F. Wang and F. C. Chang, *Macromolecules*, 2006, **39**, 5458.
16 W. C. Chen, S. W. Kuo, U. S. Jeng and F. C. Chang, *Macromolecules*, 2008, **41**, 1401.
17 W. C. Chen, S. W. Kuo, C. H. Lu and F. C. Chang, *Macromolecules*, 2009, **42**, 3580.
18 I. H. Lin, S. W. Kuo and F. C. Chang, *Polymer*, 2009, **50**, 5276.
19 C. H. Lu, S. W. Kuo, W. T. Chang and F. C. Chang, *Macromol. Rapid Commun.*, 2009, **30**, 2121.
20 S. C. Chen, S. W. Kuo, U. S. Jeng and F. C. Chang, *Macromolecules*, 2010, **43**, 1083.
21 N. V. Salim, T. Hanley and Q. Guo, *Macromolecules*, 2010, **43**, 7695.
22 N. V. Salim, N. Hameed and Q. Guo, *J. Polym. Sci., Part B: Polym. Phys.*, 2009, **47**, 1894.
23 N. Hameed, N. V. Salim and Q. Guo, *J. Chem. Phys.*, 2009, **131**, 214905.
24 M. A. Hillmyer, P. M. Lipic, D. A. Hajduk, K. Almdal and F. S. Bates, *J. Am. Chem. Soc.*, 1997, **119**, 2749.
25 P. M. Lipic, F. S. Bates and M. A. Hillmyer, *J. Am. Chem. Soc.*, 1998, **120**, 8963.
26 Y. Huang, J. Yang, H. Cai, Y. Zhai, D. Feng, Y. Deng, B. Tu and D. Y. Zhao, *J. Mater. Chem.*, 2009, **19**, 6536.
27 F. Liu, C. Li, L. Ren, X. Meng, H. Zhang and F. S. Xiao, *J. Mater. Chem.*, 2009, **19**, 7921.
28 X. Zhuang, Y. Wan, C. M. Feng, Y. Shen and D. Y. Zhao, *Chem. Mater.*, 2009, **21**, 706.
29 C. Z. Yu, J. Fan, Z. B. Tian and D. Y. Zhao, *Chem. Mater.*, 2004, **16**, 889.
30 Y. H. Deng, T. Yu, Y. Wan, Y. F. Shi, Y. Meng, D. Gu, L. J. Zhang, Y. Huang, C. Liu, X. J. Wu and D. Y. Zhao, *J. Am. Chem. Soc.*, 2007, **129**, 1690.
31 H. Kosonen, J. Ruokolainen, P. Nyholm and O. Ikkala, *Polymer*, 2001, **42**, 9481.
32 H. Kosonen, J. Ruokolainen, P. Nyholm and O. Ikkala, *Macromolecules*, 2001, **34**, 3046.
33 S. Valkama, A. Nykanen, H. Kosonen, R. Ramani, F. Tuomisto, P. Engelhardt, G. ten Brinke, Okkala and J. Ruokolainen, *Adv. Funct. Mater.*, 2007, **17**, 183.
34 D. Hu, Z. Xu, K. Zeng and S. Zheng, *Macromolecules*, 2010, **43**, 2960.
35 J. G. Li, Y. D. Lin and S. W. Kuo, *Macromolecules*, 2011, **44**, 9295.
36 S. W. Kuo, C. L. Lin and F. C. Chang, *Macromolecules*, 2002, **35**, 278.
37 D. Patterson, *Polym. Eng. Sci.*, 1982, **22**, 64.
38 H. Zhang, D. E. Bhagwagar, J. F. Graf, P. C. Paitner and M. M. Coleman, *Polymer*, 1994, **35**, 5379.
39 W. H. Jo, Y. K. Kwon and I. H. Kwon, *Macromolecules*, 1991, **24**, 4708.
40 S. W. Kuo, S. C. Chan, H. D. Wu and F. C. Chang, *Macromolecules*, 2005, **38**, 4729.
41 S. W. Kuo, *J. Polym. Res.*, 2008, **15**, 459.
42 J. Wei, Y. Deng, J. Zhang, Z. Sun, B. Tu and D. Y. Zhao, *Solid State Sci.*, 2010, **13**, 784.
43 Y. Deng, J. Liu, C. Liu, D. Gu, Z. Sun, J. Wei, J. Zhang, L. Zhang, B. Tu and D. Y. Zhao, *Chem. Mater.*, 2008, **20**, 7281.
44 C. F. Huang, S. W. Kuo, H. C. Lin, J. K. Chen, Y. K. Chen, H. Y. Xu and F. C. Chang, *Polymer*, 2004, **45**, 5913.
45 J. Shen and S. X. Zheng, *J. Polym. Sci., Part B: Polym. Phys.*, 2006, **44**, 942.
46 X. Li, L. Song and B. D. Vogt, *J. Phys. Chem. C*, 2008, **112**, 53.
47 S. W. Kuo and F. C. Chang, *Prog. Polym. Sci.*, 2011, **36**, 1649.
48 Y. Qin, H. Ren, F. Zhu, L. Zhang, C. Shang, Z. Wei and M. Luo, *Eur. Polym. J.*, 2011, **47**, 853.
49 I. Nischang, O. Brggemann and I. Teasdale, *Angew. Chem., Int. Ed.*, 2011, **50**, 4592.
50 L. Zhang, H. C. L. Abbenhuis, Q. Yang, Y. M. Wang, P. C. M. M. Magusin, B. Mezari, R. A. van Santen and C. Li, *Angew. Chem., Int. Ed.*, 2007, **46**, 5003.
51 B. H. Yang, H. Y. Xu, Z. Z. Yang and X. Y. Liu, *J. Mater. Chem.*, 2009, **19**, 9038.
52 H. C. Lin, S. W. Kuo, C. F. Huang and F. C. Chang, *Macromol. Rapid Commun.*, 2006, **27**, 537.
53 M. W. Huang, S. W. Kuo, H. D. Wu, F. C. Chang and S. Y. Fang, *Polymer*, 2002, **43**, 2479.
54 C. F. Huang, S. W. Kuo, F. J. Lin, W. J. Huang, C. F. Wang, W. Y. Chen and F. C. Chang, *Macromolecules*, 2006, **39**, 300.
55 C. Y. Chiu, W. H. Hsu, Y. J. Yen, S. W. Kuo and F. C. Chang, *Macromolecules*, 2005, **38**, 6640.
56 S. W. Kuo, S. C. Chan and F. C. Chang, *J. Polym. Sci., Part B: Polym. Phys.*, 2004, **42**, 117.
57 S. W. Kuo, C. F. Huang and F. C. Chang, *J. Polym. Sci., Part B: Polym. Phys.*, 2001, **39**, 1348.
58 S. W. Kuo, W. J. Huang, C. F. Huang, S. C. Chan and F. C. Chang, *Macromolecules*, 2004, **37**, 4164.
59 S. W. Kuo, W. P. Liu and F. C. Chang, *Macromol. Chem. Phys.*, 2005, **206**, 2307.
60 K. W. Huang, L. W. Tsai and S. W. Kuo, *Polymer*, 2009, **50**, 4876.
61 H. L. Chen, S. C. Hsiao, T. L. Lin, K. Yamauchi, H. Hasegawa and T. Hashimoto, *Macromolecules*, 2001, **34**, 671.
62 H. L. Chen, J. C. Wu, T. L. Lin and J. S. Lin, *Macromolecules*, 2001, **34**, 6936.
63 Y. L. Loo, R. A. Register, A. J. Ryan and G. T. Dee, *Macromolecules*, 2001, **34**, 8968.
64 J. T. Xu, S. C. Turners, J. P. A. Fairclough, S. M. Mai, A. J. Ryan, C. Chaibundit and C. Booth, *Macromolecules*, 2002, **35**, 3614.
65 J. Y. Hsu, I. F. Hsieh, B. Nandan, F. C. Chiu, J. H. Chen, U. S. Jeng and H. L. Chen, *Macromolecules*, 2007, **40**, 5014.
66 M. M. Coleman, J. F. Graf and P. C. Painter, *Specific Interactions and the Miscibility of Polymer Blends*, Technomic Publishing, Lancaster, PA, 1991.
67 M. M. Coleman and P. C. Painter, *Miscible Polymer Blend-Background and Guide for Calculations and Design*, DEStech Publications, Inc., 2006.
68 W. D. Harkins and G. Jura, *J. Am. Chem. Soc.*, 1944, **66**, 1366.
69 J. G. Li and S. W. Kuo, *RSC Adv.*, 2011, **1**, 1822.
70 K. S. W. Sing, D. H. Everett, R. A. W. Hual, R. A. Pierotti, J. Rouquerol and T. Siemieniewska, *Pure Appl. Chem.*, 1985, **57**, 603.
71 D. Y. Zhao, Q. S. Huo, J. L. Feng, B. F. Chmelka and G. D. Stucky, *J. Am. Chem. Soc.*, 1998, **120**, 6024.
72 F. Kleitz, S. H. Choi and R. Ryoo, *Chem. Commun.*, 2003, 2136.
73 H. F. Yang and D. Y. Zhao, *J. Mater. Chem.*, 2005, **15**, 1217.